CHAPTER ONE

INTRODUCTION

Pulsars are rapidly-rotating, highly-magnetized neutron stars radiating predominantly linearly polarized electromagnetic radiation. The radiation region is confined to a narrow cone around its magnetic field axis. Depending on the alignment of the observer, the magnetic axis and the axis of pulsar rotation, the radiating cone sweeps across the line of sight of the observer periodically, much like a rotating beacon (for more details see Ruderman et. al., 1975). This results in a periodic train of narrow pulses of broad-band radiation, which can be detected using a radio telescope. During the past thirty years since the discovery of the first pulsar, several searches for pulsars have been conducted resulting in detection of about 700 pulsars. A large number of these pulsars have been studied at various radio frequencies and form the basis for our present understanding of their characteristics. Different types of observable parameters, such as the pulse periodicity, its rate of change, the pulse width, pulse energy, pulse shape and its structures, polarization of radiation received at different positions within the pulse, and their spatial and temporal variations are of great interest, besides the characterization of some of the properties of interstellar medium through which the pulsar signal propagates. The signal processing for detection and analysis of pulsar signals is quite complex, imposing the need for a high computational throughput, typically of the order of a few Giga operations per second. This thesis describes the design, tests and results of a real-time signal processing instrument built to aid in the search and study of pulsars. In this context, it is useful to discuss the general characteristics of pulsar signals.

1.1 General Characteristics of Pulsar Signals

Some of the basic observational properties of pulsar signals are as follows:

1.1.1 Pulse period:

All pulsars show emission of broad-band radio noise in the form of periodic train of pulses with periods ranging between ≈ 1.5 msec and about 4 sec. The arrival times of these pulses are extremely stable to a precision better than 1 part in 10^7 over intervals of a few months, (Hewish et. al., 1968) and on a short time scale, the arrival time shows only a small jitter that averages out over a few hundred pulses. Although the pulse energy from most pulsars is confined to a small window within a period, some exceptions exist where an additional pulse component, called the *interpulse*, is situated approximately half-way between the main pulses. The interpulses are interpreted as the radiation from the opposite pole of the pulsars, and in these cases, the axis of rotation and the axis of the radiating poles have to be in a geometry such that the observer receives the radiation from both the poles as it rotates. In almost all the cases, the shape and intensity of the main and the interpulse are not identical. The period of all pulsars is found to be lengthening at a constant rate

(Gold, 1968), and for some pulsars, the period suddenly switches to a shorter period (Radhakrishnan, 1969. Lohsen, 1975, and Manchester et. al., 1976) and continues to lengthen thereafter. The lengthening of the period is related to the gradual slowing down of the rotation of the pulsar.

1.1.2 Pulse Shape:

Every pulsar has a unique profile that is stable when averaged over many periods. Average profiles of pulsars show complex pulse structures, many of them with several components and identifiable peaks (see for example, Rankin 1981). Individual pulses are often found to be made up of two or more sub-pulses which may vary in their position and some of them showing a systematic drift within the pulse (Drake and Craft. 1968; Taylor et. al., 1975; Backer. et. al., 1975). There is also some microstructure that has a characteristic width of about 10 to 100μsec (Manchester and Taylor, 1977). The shapes of the integrated profiles are frequency-dependent.

The width of a pulse is difficult to define due to complex variations in the shape of the profile. A more common term used is the *equivalent width,* defined as the ratio of the pulse energy and the peak flux density. Observed equivalent widths for presently known pulsars vary from about a few msecs to a few hundred milliseconds. Although there is considerable scatter in the data, the pulse widths vary with period and the mean duty cycle is about 3%.

1.1.3 Pulse Energy:

Pulse intensities may vary with time and in some pulsars the pulses vanish for several periods (a phenomenon called nulling) (Ritchings 1976, Backer 1970, Hesse and Wielebinski, 1974). Irrespective of the nulling effect, the pulses appear in a highly periodic sequence. The average pulse intensity depends on the observing frequency, and this dependence is well described by a power-law with a spectral index a defined by

$$S = S_o f^{\alpha} \tag{1.1}$$

Where S is the flux density and f is the frequency. This index is usually around -1.5, indicating a steep dependence. For most pulsars the spectrum becomes steeper in the region 100 to 500 MHz and a spectral maximum is observed around 100 MHz (Comella 1972, Bruck et. al. 1978). At much lower frequencies observations are hindered due to interstellar absorption and distortions of the pulse shapes due to interstellar scattering. Also the ionosphere becomes reflective at frequencies below 10MHz and sets a lower limit to the observable radiation from ground based telescopes.

1.1.4 Polarization:

One of the striking properties of pulsars is the high degree of polarization of their radiation. The integrated profiles of a number of pulsars show nearly complete linear polarization. The polarization angle of the linearly polarized component shows a systematic sweep across the pulse (Radhakrishnan and Cooke 1969). Circular polarization is also observed but in an integrated profile it very rarely exceeds 20 percent of the total intensity. However, pulsars with drifting sub-pulses show weakly polarized integrated profiles. It was observed that the polarization of some pulsars switches to a new stable value at irregular intervals of a few hours (Backer 1970, Hesse 1973). The pulsar remains in this state for several hundreds of periods before abruptly returning to its original stable state. This effect is popularly called polarization mode - changing. The fractional polarization of integrated pulsar profiles has been observed to decrease with increasing frequency.

1.2. Propagation Effects on Pulsar Signals:

Pulsar signals travel typically tens of thousands of light years during the journey before they reach the telescope. During this journey, the pulsar signals pass through the interstellar medium. interplanetary medium and the Earth's ionosphere. Presence of ionized regions and magnetic field in this intervening medium produces distortions in the pattern of the original profile. This distortion is related to the spatial distribution of electron density and strength of the magnetic field in the medium in the observer's line of sight. The different ways in which the medium affects the signal may be identified as follows:

1.2.1. Dispersion:

The propagation time for an EM wave of a frequency f in a plasma region through a column of length 'L' and average electron density N is given (Manchester and Taylor, 1977) by

$$\tau_\lambda = \frac{L}{c}\left(1 + \frac{e^2 N}{2\pi m f^2}\right) \quad \text{sec} \tag{1.2}$$

Where e = charge of an electron

m = rest mass of an electron

and c = velocity of light

Generally, the observed bandwidth is limited by the receiver front-end with the lower and upper edge frequencies being, say, f_{low} and f_{high} respectively. At any frequency f within this band, the difference in arrival time relative to the signal at f_{high} is given by

$$\Delta\tau = \frac{L}{c}\left[\frac{e^2 N}{2\pi m}\right]\left[\frac{1}{f^2} - \frac{1}{f_{high}{}^2}\right] \tag{1.3}$$

Where f is in Hz.

Substituting values for standard constants

$$\Delta\tau = 4150 . DM . \left[\frac{1}{f^2} - \frac{1}{f_{high}{}^2}\right] \tag{1.4}$$

Where DM (dispersion measure) depends upon the interstellar electron density n_e and the distance to the pulsar, given by

$$DM = \int_0^L n_e dl \tag{1.5}$$

Thus, the delay at different frequencies within the observing band is different (inversely proportional to the square of the frequency), and this gives rise to a time-smearing of the true pulse profile. Hence the observed pulse width will be larger than that of the intrinsic profile by $\Delta\tau$. Figure(1.1) displays the time-frequency pattern of a dispersed pulsar profile. This expansion in the pulse width Pw is accompanied by a corresponding reduction in the pulse height, since pulse energy is conserved. This effect has two disturbing consequences. Firstly, the reduction in pulse height worsens the signal to noise ratio (SNR) thereby reducing the detection sensitivity. Secondly, the time smearing across the pulse smoothes out finer details within the pulse.

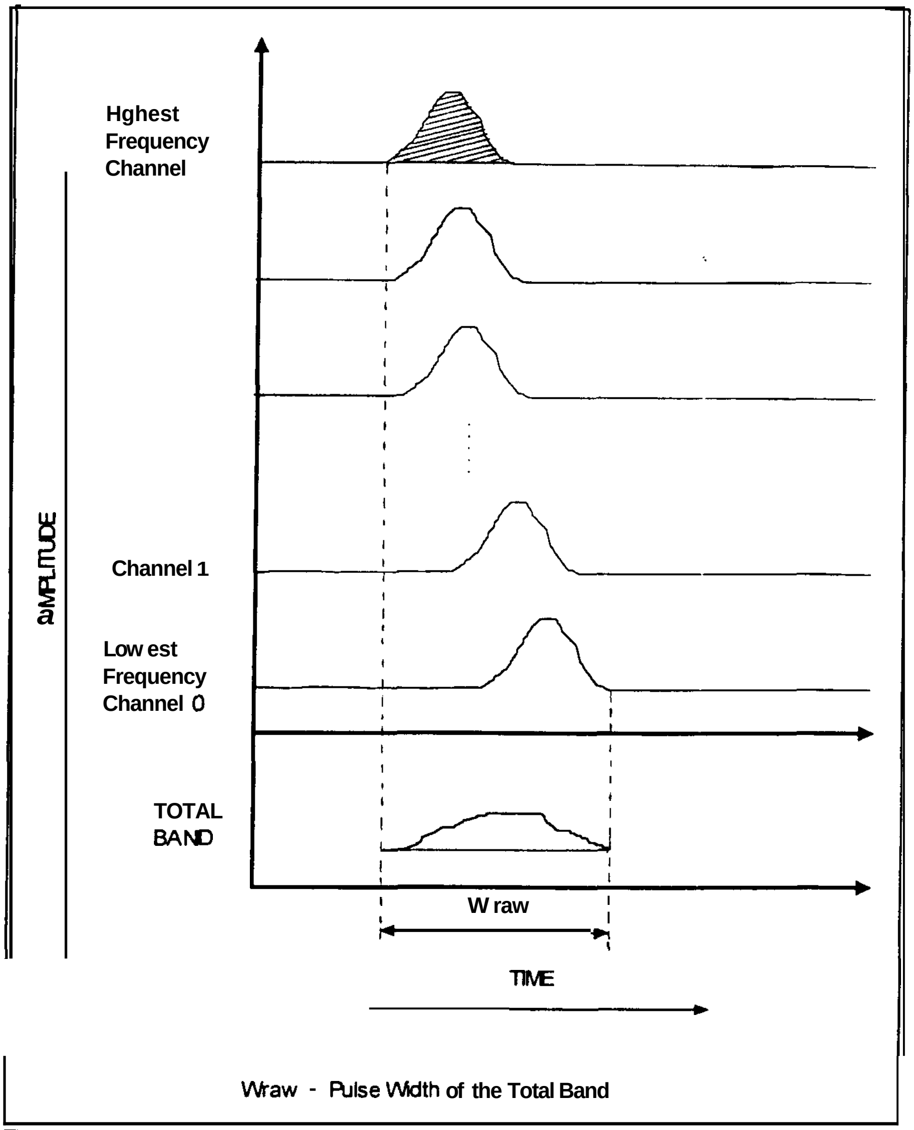

Fig. 1.1 Pulse Profiles at various frequencies within the observed band-width in presence of dispersion (the bottommost profile shows pulse smearing w hen the total band is collapsed to one channel).

To avoid these effects, the delay gradient in arrival time across the observing band has to be modeled accurately and corrected. Sutton proposed a scheme using swept frequency local oscillators (Sutton et. al., 1970) in which the local oscillator frequency would be swept in a direction opposite to the time-frequency curve produced by the dispersive delay gradient. The characteristics may vary with a number of environmental factors such as temperature, noise and ripples in power supplies, etc. The option of implementing the desired correction using a digital filter is the standard practice presently. Two methods, called incoherent and coherent de-dispersion, are commonly employed. In coherent method, the raw samples of the digitized data will be convolved with a transfer function is the complex conjugate of that of the dispersion function (Hankins, 1971). However, this will require a filter bearing a large number of taps and corresponding coefficients, since the resolution is equal to the sampling interval and the number of taps should hold data over a time length equal to the total dispersion delay across the band. This scheme is presently used in cases when the bandwidth is small (about a MHz) and the observing frequency is reasonably high, about a few GHz. Also, many types of pulsar observations do not require very high time resolution. For such observations the incoherent de-dispersion method (Hankins and Rickett. 1975) is usually employed. In this method, the sampled data is initially digitized and Fourier transformed to produce power spectrum over the given band width, with a number of frequency channels that give the required frequency resolution. The spectra of consecutive time frames form a 2-d matrix of frequency and time as shown in figure (1.1).

The arrival time delay in each frequency channel with respect to that in the highest frequency channel, is calculated in units of new sampling interval as

$$\Delta n = \frac{\Delta\tau}{T_{frame}} \tag{1.6}$$

Where T_{frame} is the time interval between consecutive frequency spectra. To compensate for this arrival time difference, the data of the individual frequency channels are delayed suitably with respect to that in the lowest frequency channel in the band employing digital storage delay lines. This form of correction is illustrated in figure (1.2).

This method corrects for dispersion between channels but ***not*** within the channels. The uncorrected smoothing increases in the lower frequency channels, with the maximum error being in the lowest frequency channel, given by

$$\mathrm{Max}(\Delta\tau_{err}) = 4150\,DM\left[\frac{1}{f_{low}^{\;2}} - \frac{1}{(f_{low}+\Delta f_{chan})^2}\right] \tag{1.7}$$

where Δf_{chan} is the bandwidth per spectral channel.

Due to this fact, the error can be corrected with better resolution by increasing the number of frequency channels within a given band, such that the bandwidth per channel is reduced. However, this resolution cannot be enhanced indefinitely. For a given channel bandwidth, the channel automatically imposes a time constant $\Delta\tau_{chan}$, within which the signal is averaged by the channel itself and the details of variations faster than this time constant will be smoothed out. As the channel bandwidth is reduced, this time constant increases. Thus, for a given operating frequency, the optimal bandwidth is decided by two opposing factors - the dispersion delay and channel response time (another limiting factor - scattering in the interstellar medium, poses the ultimate limit, this will be discussed later):

$$\Delta\tau^2 tot = (\Delta\tau_{disp}{}^2 + \Delta\tau_{chan}{}^2) \quad (1.8)$$

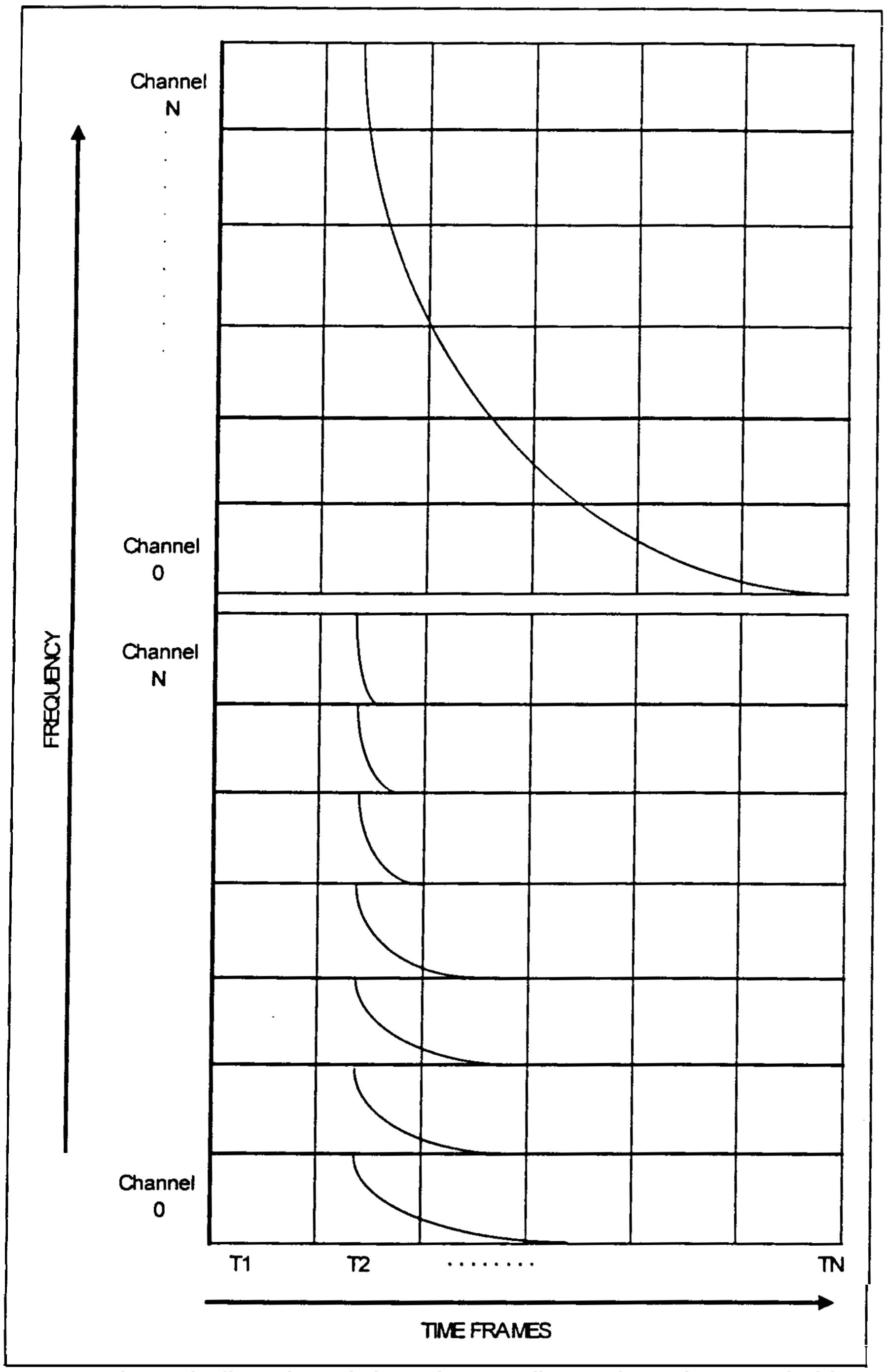

Fg. 1.2 Incoherent de-dispersion technique. The upper diagram shows the raw arrival time delay gradient across the band; the bottom portion represents it after incoherent de-dispersion (also indicating the residual delays within each channel.

The minimum smearing is when the two factors are equal. Then the optimal channel bandwidth can be related to these factors as (Deshpande, 1989)

$$\Delta f_{ch\_opt} \approx \frac{1}{91}\sqrt{\frac{f_o^{\,3}}{DM}} \tag{1.9}$$

Once the optimal channel bandwidth is chosen, the FFT is performed over suitable number of time samples so as to produce the number of channels that cover the total receiver bandwidth.

1.2.2. Faraday Rotation:

As mentioned earlier, pulsars are sources of predominantly linearly polarized radiation. The frequency dependency of the apparent position angle of the polarization is of importance in estimating the amount of Faraday rotation in the intervening medium. Due to the presence of ionized plasma and magnetic field in the interstellar medium and the ionosphere, Faraday rotation takes place predominantly in ISM & ionosphere. If the original pulsar radiation had a polarization angle Φ at a longitude L of the pulsar at a wave length λ then the observed polarization angle is

$$\Phi obs_{(L,\lambda)} = \Phi orig_{(L,\lambda)} + \theta \tag{1.10}$$

where

$$\theta = \frac{e^3 \lambda^2}{8\pi^2 c^3 \varepsilon_0 m^2} \int_0^R N\,B\,Cos(\psi)\,dr \tag{1.11}$$

Where $B.\,Cos(\psi)$ is the magnetic field component along the line of sight, Ψ being the angle between the magnetic field lines and the line of sight of the observer, N is the electron density in the line of sight and R is the distance to the pulsar. If R is in Parsecs. N is in cm^{-3}, B is in Gauss and A in m, substituting the constants we get

$$\theta = \lambda^2 \left[8.1x10^5 \int_0^R NB\cos(\psi)\,dr \right] \tag{1.12}$$

Usually this is represented as $\theta = RM.\,\lambda^2$, where RM is the term within brackets, called the "rotation measure" expressed in Rad, m^{-2}. The rotation of the polarization angle is a function of the magnetic flux density in the line of sight, the column density of electrons in the interstellar medium and the wavelength A. The polarization vector rotates within the receiver bandwidth and is more rapid at lower observing frequencies. The rate of rotation given by the function

$$\frac{d\theta}{df} = \frac{d}{df}\left[\frac{RMc^2}{f^2}\right] = -\left[\frac{2RMc^2}{f^3}\right] \tag{1.13}$$

Where c is the velocity of light.

Thus at lower observing frequencies the spectral components of pulsar radiation will add up vectorially with different polarization angles, causing depolarization. Usually the circular and linear polarized components filtered out separately by computing the time averaged Stokes parameters (V and Q+jU respectively). If the RM is known, then. for a given operating frequency band. this rotation can be corrected by computing and subtracting the Faraday rotation from the linear components at various frequencies within the band. Usually the signal is Fourier transformed to get the frequency spectra with several frequency channels and the differences in Faraday rotation in each channel is corrected relative to that at one of the edge channels of the band. This type of correction accounts for the differential rotation between channels, but leaves the rotation within each channel uncorrected. For a finite number of channels of bandwidth Δf_{chan}, the residual smearing of polarization angle within the channels (after correction between channels) will extend over a range

$$\Delta\theta = \frac{d\theta}{df} \times \Delta f = -\left[\frac{2RMc^2}{f_0^{\ 3}}\right]\Delta f_{chan} \qquad (1.14)$$

Where f_0 is the center frequency of the channel. Naturally, this smearing will be maximum in the lowest frequency channel of the band. The correction accuracy improves by splitting the band into more number of frequency channels, but the number cannot be increased arbitrarily. Apart from practical limitations in producing a large number of frequency channels, there are many factors that distort the polarization information and unfortunately, they can be only estimated and not corrected. For example, there are turbulences in the ionosphere which introduces random and rapid changes in the electron density in the line of sight of the observer (Spoelstra and Kelder, 1984). Also, the waves reflected from the ground will have random rotations in polarization and when superposed with the direct ray picked by the antenna they cause depolarization (this also changes with time as the antenna tracks the source). Besides this, the complex gains of the receivers and the leakage between the two orthogonal polarization channels may also fluctuate with time, introducing spurious polarization. Typically, the ambiguity due to these random components limits the accuracy of determination of the polarization angle of ground based radio telescopes to a few degrees.

1.2.3. Interstellar Scattering:

The interstellar plasma through which the pulsar signal propagates is in homogeneous, consisting of electron density fluctuations of various scales. This causes irregular changes in the propagation direction, resulting in scattering of the signal (Manchester and Taylor 1977, Sutton 1971). When a wave of frequency f passes through a layer of interstellar medium located at distance 'd' from the observer with an irregularity An, in its electron density over a scale size 'a', the wave front bends by an amount

$$\theta_{scat} \approx \left[\frac{e^2 \Delta n_e}{2\pi f^2 m_e}\right]\sqrt{\frac{d}{a}} \qquad (1.15)$$

In general the density fluctuations are random and generate a Gaussian distribution of scattering angles with scale $\theta_{sc.}$ Due to this, the observer receives the signal not only along the direct path from the pulsar but also along the scattered path. Since the scattered paths are longer than the direct path the signal arriving through these paths are delayed replica of that in the direct path. At the receiver the superposition of all these signals results in broadening of the trailing edge of the pulse and smooth out the details of original structures within the pulse. This smearing of the pulse depends on the distance, electron density, and the scale size 'a' as

$$\Delta t_{scat} = \left[\frac{d}{c}\right]\theta_{scat}^{\ 2} \qquad (1.16)$$

The smearing increases sharply with the wavelength of observation and the dispersion measure (Ramachandran et. al., 1997). At low frequencies, the scatter-broadening will dominate the time smearing produced by dispersion. Since the scattering is a random process the time smearing may only be estimated but cannot be corrected unlike in the case of dispersion effects.

Another effect of scattering is scintillation. Since the arrival time of the rays along different paths are not identical, the signals interfere with each other at the receiving antenna. For a given scale size of irregularities in the interstellar medium between the pulsar and the observer. These interfering rays produce a corresponding diffraction pattern in both frequency and space. Across a given observing band-width the scintillations show up as random intensity modulations across the power spectrum. Also the net intensity received by the receiver may fluctuate with time as the earth moves and traces different portions of the diffraction pattern in space. While the frequencies structure of scintillations contributes extra noise to the power spectrum, the time dependent variations are more difficult to account for.

1.3. Effects Due to Motion of the Earth and Pulsar:

1.3.1. Period Changes:

The rotation and orbital motion of the earth, the motion of the solar system and the pulsar will result in a complex motion of observer's platform with respect to the pulsar. Some of the components of this relative motion are as follows:

1. Earth rotation velocity
2. Earth orbit around solar system barry-centre
3. Motion of the solar system around the galactic center
4. Proper motion of the pulsars in the galaxy and

5. If the pulsar is a member of a binary system, then its velocity & acceleration along the line-of-sight of the observer due to orbital motion.his relative motion introduces Doppler shift in the received pulse frequency which changes with time as the relative velocities and accelerations change. Elaborate calculations are available (Manchester and Taylor, 1977) for modeling the observed period of the pulsar at a given time t, taking into account the above factors. Standard software routines are also available for estimation of the observed period at any given epoch for all pulsars. Once the observer's position, the pulsar position and the observation's epoch are precisely known, using these routines, the changes in the period can be estimated. For some pulsar observations, it is necessary to fold the pulses over its period to improve the signal to noise ratio of the profile (explained in chapter 2). In such cases, the pulse profile should remain matched in phase as the folding progresses, otherwise the successive pulses do not add coherently and lead to reduction in S/N ratio and also smoothes away details of fine structures in the pulse profile (as shown in figure (1.3).). It is required that the change in period be estimated on-line and for a given sampling rate, the phase increment per sample is scaled correspondingly so as to fold the pulses synchronously over the period.

1.3.2. Changes in Apparent Linear Polarization Angle (Parallactic Angle):

The measured polarization position angle of pulsar radiation has to be referred to a standard co-ordinate system in order to represent the angle in same units independent of the alignment of the polarization plane of the antennas and the plane of the wave front. By convention, this reference plane is taken as the plane containing the N-S poles. For a given position of the source and the Alt-Az- mount telescope, the alignment of the polarization angle of the wave and the antenna changes as the earth rotates, depending upon the hour angle of the source. This observed change is called the parallactic angle. For a given latitude (L) of the observatory, the declination (δ) of the source, and for an alt-az mount it is expressed as (VLA,R.M Hjellming).

$$\theta_{par} = \tan^{-1}\left[\frac{\mathrm{Cos(L).Sin(HA)}}{\mathrm{Cos}(\delta)\mathrm{Sin(L)} - \mathrm{Cos(L)Sin}(\delta)\mathrm{Cos(HA)}}\right] \qquad (1.17)$$

Where HA is the Hour Angle of the source (the angular distance between the observer's longitude and the source). This change in the observed polarization angle is purely a "local" geometrical effect and has nothing to do with any changes in the intrinsic nature of the incident wave, and is same at all frequencies within the observed band. Parallactic angle has to be subtracted from the observed linear polarization angle so as to remove the instrumental effect in the sweep of polarization angle.

1.4 Instrumental Stability and Accuracy:

Several factors associated with the telescope and its instruments affect the sensitivity, accuracy and repeatability of the measurements considerably. In this section instrumental effects of concern with radio telescopes having arrays of antennas will be discussed with special relevance to the GMRT telescope.

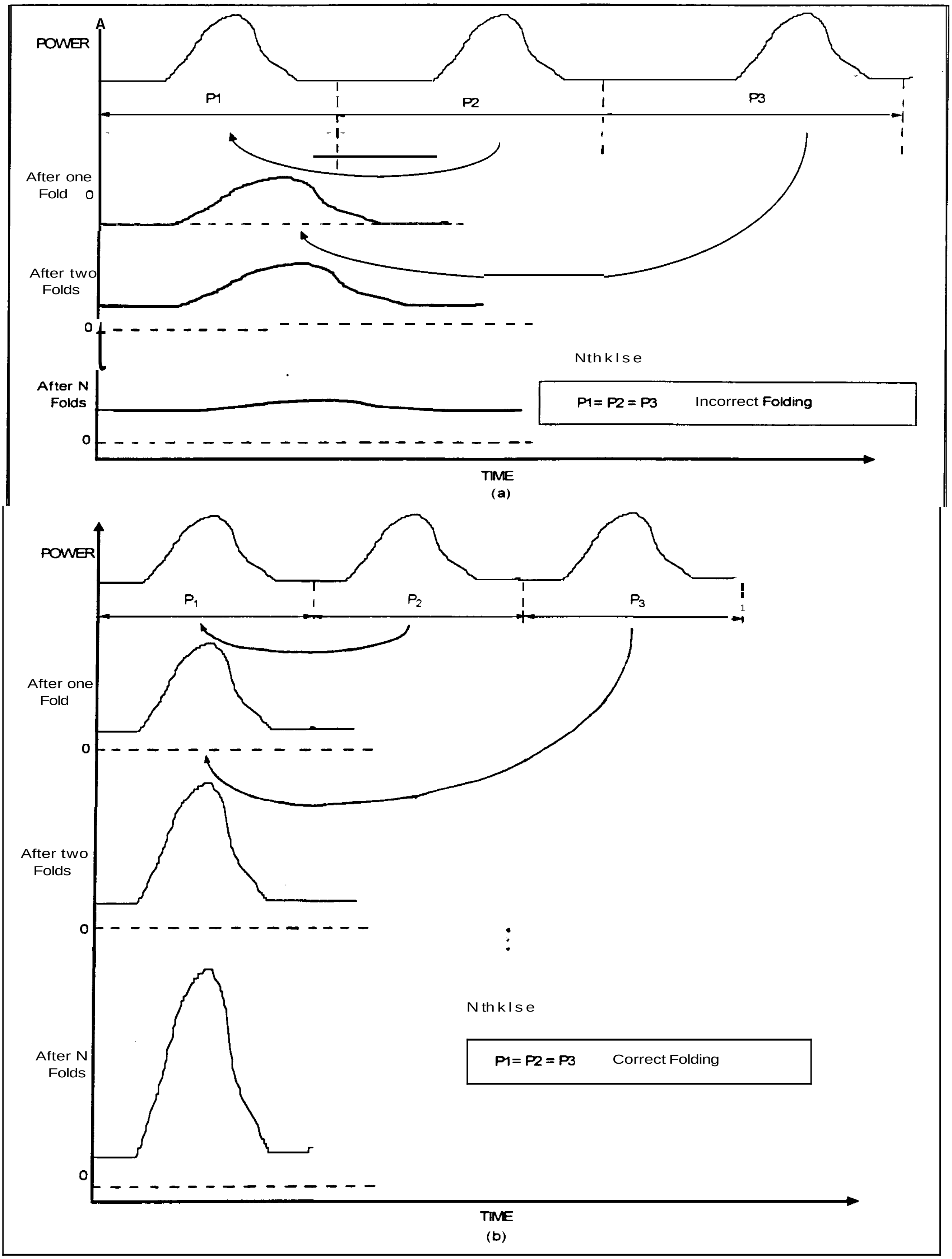

Fig 1 3 The pulse profile smoothens out ▮ the folding period is wrong as shown in (a) while,the pulse grows in signal to noise ratio by folding with correct period as shown in (b) a). Any deviations in the shape of the reflecting surface of the antenna from that of a parabolic will result in change in its polarization response and can lead to distortion of the polarization of the received signal. Usually changes in the shape of the surface occur due to deformations under gravity. This may also happen when the reflecting surface is hit with winds of high velocity. The loss of accuracy in polarization measurement can only be estimated with repeated calibration observations but cannot be recovered.

b). In arrays of antennas the feeds at the focus of individual antennas may not be aligned exactly with each other. Thus when the signals from all the antennas combine the vectorial components of polarization from different antennas differ from each other in their polarization angles and add up inhomogeneously producing depolarization. This depolarization can be minimized by proper alignment of feeds in the array.

c). The electrical phase difference between the two orthogonal polarization channels of an antenna plays a crucial role in the estimation of stokes parameters. In case of circularly polarized channels, if e_l, e_r are the complex voltages developed in the left and right circular feeds of the antenna and a phase difference ζ is introduced in the receiver, then

$$Q + jU = e_l \cdot e^{j\zeta} \cdot e_r^* \tag{1.18}$$

This will result in only an additional tilt in the linear polarization angle and does not affect the linear intensity or the circular intensity. However if the receiver used two orthogonal linearly polarized channels which produced voltages e_x, e_y, then any phase difference introduced by the receiver between the channels will affect both the linear and circular components of the signal as follows:

Linear components =

$$Q = \left(|e_x|^2 - |e_y|^2 \right) \tag{1.19a}$$

$$U = \mathrm{real}\left(2 \cdot e_x \cdot e_y^* \cdot e^{j\zeta}\right) \tag{1.19b}$$

So Q is unaffected but U is affected. This will affect both amplitude and polarization angle measured for linear component.

Circular component =

$$V = \mathrm{imag}\left(2 \cdot e_x \cdot e_y^* \cdot e^{j\zeta}\right) \tag{1.20}$$

Therefore in case of linear feeds, the phase differences also affect the intensity measured for circular component. In most receivers the phase difference arises due to differences between the receivers in the phases of local oscillators, mixers and amplifier stages and also unequal transmission line lengths. All these are complex functions of frequency and therefore the effect may vary at different frequencies with in the observed band and cause depolarization when the band is collapsed into a single channel. These effects have to be corrected before combining power from different antennas in an array. This phase difference has to be calibrated with injection of suitable test signals at the inputs of the front-end receivers or by observing standard point sources whose characteristics are known. Also, any leakage due to poor isolation between the two polarization channels will lead to cross-coupling, thereby affecting all stokes parameters. Usually the isolation is designed to be sufficient to make the cross coupling insignificant.

c). Quantization noise: in most of the modern receiver back-ends the signals are processed digitally after obtaining quantized samples from the input analog signal by using suitable A/D converters. Due to finite precision in numerical representation, the quantization process introduces some error in the amplitude and phase measurements . This uncertainty propagates throughout the ensuing signal processing calculations and in particular sets a limit to the accuracy of Stokes parameter obtained. The error is a non-linear function of the number of bits chosen. For pulsar signal detection, usually only one or two bits will suffice to represent the total power from the receiver, while for full polarization pulsar studies, more number of bits are chosen such that the error is far less compared to the random fluctuations in the received signal.

1.5. Types of Pulsar Observations

Pulsar observations can be broadly classified into two major categories: those intended to discover unknown pulsars and those intended for deep studies of known pulsars or to use pulsars as probes for the intervening interstellar medium.

1.5.1 Pulsar Search Observations:

Increasing the size of the known pulsar population is important for improving statistical significance in various possible tests of many theoretical predictions and models relating to birth and evolution of neutron stars, etc. However, the pulsars generally are very weak and distant sources and their signals get scattered and dispersed during propagation through the ISMs. This effect gets worse as one looks into the plane of the galaxy, especially towards the galactic center, since the electron density of the ISM increases drastically. Owing to all the challenges it poses in instrumentation and signal processing to detect the faint pulsar signals, the number of pulsars discovered so far using the biggest telescopes of the world is only about 700. Typical sensitivity levels of pulsar surveys have been about one mJy (1Jy = 10 -26 Wm-2Hz-1). Some of the characteristics of the instrument that set a limit to the sensitivity of detection are the observing bandwidth, collecting area of **a** telescope, the noise temperature at the front-end of the receivers and of course, the time over which the signals are coherently integrated. These are discussed in detail in chapter 2. With the GMRT and ORT, multi-frequency pulsar surveys can reach sensitivity levels of about 0.2 – 0.5 (ORT 2mJy) mJy.

1.5.2. Observations for Studies of Pulsars and ISM:

Different types of studies are possible by observing the variety of characteristics of received pulse profiles. Some of the basic observables include rotational parameters of the pulsar. pulse energy, pulse shapes. polarization properties and changes in these with time & frequency.

The pulse polarization studies have been used in modeling the pulsar magnetic field geometry and have provided important clues for understanding the radiation mechanism (Radhakrishnan & Cooke, 1969; Huguenin et. al., 1971; Backer, 1976; Rankin, 1983a, 1983b; Radhakrishnan and Rankin, 1990; Lyne and Manchester. 1988). Temporal variations such as mode changes, nulling, drifting, etc. are useful in studying the details of the emission from pulsars. Pulsars with known polarization properties can be observed to detect and model the galactic magnetic field and the ionosphere. In Chapter 5, a new scheme for using pulsars as a probe of the Earth's ionosphere and the interstellar medium is presented. With GMRT, it will be possible to conduct polarization studies with a resolution in polarization angle of a few degrees and a frequency resolution of a few KHz with bandwidths of 32 MHz, simultaneously at multiple operating frequencies ranging from 1.4 GHz to 38 MHz.

The measurements of pulse periods are used in many ways. As mentioned earlier, some pulsars just "null" for several time periods and some relatively young pulsars may change (glitch) to new stable period. These are of interest in studies of the radiation mechanism and to study the interior structure of the neutron star respectively. Systematic slowing down of pulsar periods are measured and the rate of slow down is used to estimate the "age" and the surface magnetic field of the pulsar. Changes in observed period due to Doppler effect is used to find out if the pulsar is in an orbit around any other object. The period and the magnetic field along with information about the position of pulsars in our galaxy are being used for modeling the birth rate and evolution of neutron stars. Also estimates of lengthening of pulse widths due to dispersion at various frequencies is used to determine the distance to the pulsars and the electron densities of ISM in those directions. These experiments require very high stability and accuracy in the sampling intervals of the signal beside high time resolution. Typical observations require clocks with a stability of about 1 part in 10^{10}.

Measurement of the pulse energy and pulse profiles at various frequencies and its variation over different time scales are useful in many ways to understand the radiation mechanism. It also gives a measure of the spectral evolution of pulsar properties over the radiation band. Secondly, the apparent intensity distributions in time and frequency reflect the influence of the interstellar medium and can be studied to "map" the distribution of electron density (which leave their signatures on the pulsar signal in the form of dispersion, scattering and Faraday rotations) in the Galaxy.

The study of pulse shapes have found a variety of uses. In particular, it has helped in identifying and classifying the time scales of sub-pulses, micropulses and drift rates etc. and in separating pure geometrical effects from temporal effects associated with the processes that determine the pulse shape. The study of microstructure has helped in constraining the length scale of the emission regions and to estimate energy densities associated with it (Manchester and Taylor, 1977). Distortions in the intrinsic pulse shape due to dispersion and scattering can be modeled to estimate the mean electron density in the line of sight. Monitoring the shapes for several days/months yields information on the movement of interstellar clouds, their scale sizes and density.

1.6. Overview of the GMRT (Giant Meter Wave Radio Telescope):

The GMRT is located near Pune, India. Spanning over 25 Km, it consists of an array of 30 fully steerable parabolic dishes, each with a diameter of 45m (Swarup et. al, 1991). Twelve of these dishes are in a compact central array about a square kilometer in size. The remaining 18 antennas are placed along the 3 arms of a approximate 'Y'-shaped configuration with each arm extending about 14 kms from the center of array. The antennas are designed to provide multi-frequency, dual polarization operation with the help of different feeds and low noise RF amplifiers fixed on a rotatable turret at the prime focus of the parabolic reflector.

1.6.1. Front-End System:

A block diagram of the front-end system of GMRT is given in figure (1.4). The different operating

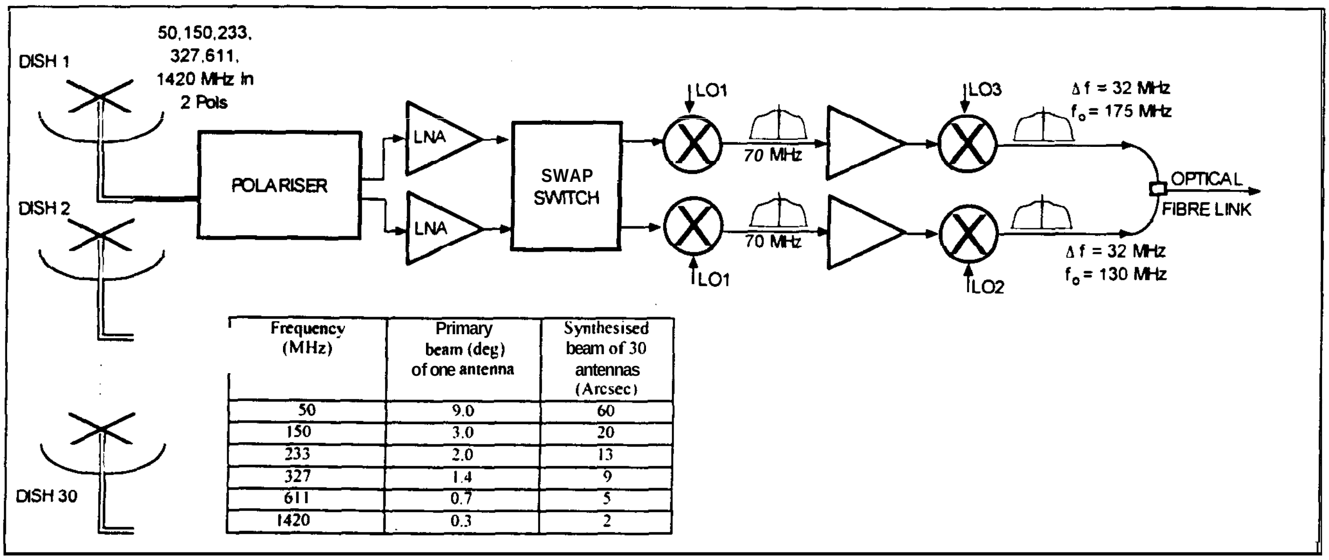

Frequency (MHz)	Primary beam (deg) of one antenna	Synthesised beam of 30 antennas (Arcsec)
50	9.0	60
150	3.0	20
233	2.0	13
327	1.4	9
611	0.7	5
1420	0.3	2

Fig. 1.4 GMRT Front End Block Diagram.The Mocks repeat for other antennas in the array.The table shows various operating frequencies and corresponding beamwidths.

frequencies of the telescope are also listed in the figure. The RF mixer stage converts the received RF-band of two polarizations to a pair of intermediate frequency bands at 135 and 170 MHz respectively. Optical fibre links are used to distribute coherent local oscillator signals to the antenna. The bandwidth at this stage is restricted to 32 MHz per polarization channel. The local oscillator frequency is chosen depending on the operating frequency of the feed on the turret, such that any of the operating frequency bands can be brought down to a fixed intermediate frequency (IF) band. Optical fibres are used to bring the IF bands from the antennas to a central laboratory.

Figure (1.5) shows a block diagram of the base-band system at the central laboratory. The signals are transported to video bands through SSB mixers. The converters also split the 32 MHz band into two sub-bands, each extending from 0 to 16 MHz. A set of programmable filters for each sub-band allow the video bandwidth to be chosen between 2,4,8,16 MHz. Signals from each antenna, polarization and sub-band are digitized and supplied to the rest of the systems at Nyquist rate. At this stage there are 120 parallel data streams corresponding to 30 dishes two polarizations and two sub-bands, each carrying data at a maximum rate of 32 mega samples per second.

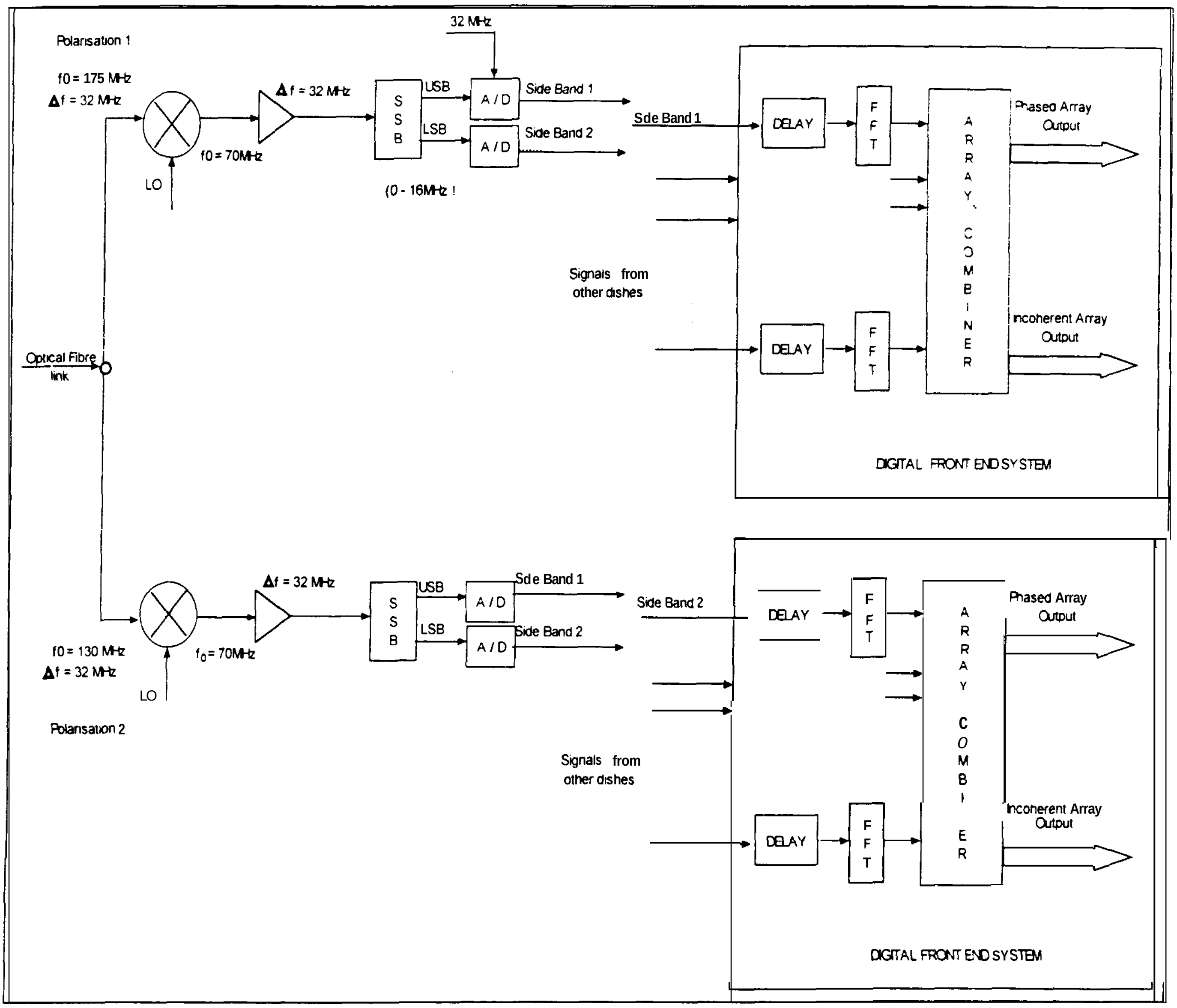

Fig 1.5 Block Diagram of GMRT baseband system shown handles signals from one antenna-theentire Mock repeats for every antenna of the GMRT array.

1.6.2. Antenna Phasing:

The arrival time differences vary from antenna to antenna and change with time since the direction changes as the antenna tracks. The data stream of each antenna, polarization and sub-band flows into individual FFT hardware modules which produce 512 point FFTs for each sub-band. The arrival time delay is compensated by memory based, digital delay lines to an accuracy of 1 sampling interval. At the output of FFT the fractional uncorrected delay (the residual delay within one sample interval after memory based correction) is compensated by multiplying the complex spectrum at the output of FFT with a suitable linear phase gradient.

1.6.3. Array Combiner (AC):

Once the array is phased properly it is required to sum up the signals of all the antenna to gain in sensitivity. The array signals is combined in two fashions (both in parallel), as explained below:

- **Pre Detection Combination:**

In this scheme the complex voltages from each antenna can be added together and then the power can be detected for further processing. In this method, the phase of the signals reaching the antennas have to be equalized before combining as mentioned earlier. The response of the combined telescope is much narrower than that of a single antenna, and there is a corresponding increase in the directive gain. Such a mode of combining the array, called as phased array (PA) mode, can be used for probing deeper in space, but over a narrow region of the sky at a given time, for example, for targeted pulsar search and pulsar studies.

- **Post Detection Combination:**

In this case, the complex signals from individual antennas are detected and their powers are combined. In this process, the significance of any phase differences between the antennas is lost and the telescope will have a beam width equal to that of a single antenna but at a reduced directive gain.This mode of operation, usually called the incoherent array (IA) mode is useful for surveying broad regions of sky, e.g., in untargeted pulsar searches. The collecting area of the telescope in PA mode is expected to be 30,000 sq.m. while in IA mode it is expected to be 5500 sq.m. (for further details, refer Deshpande, 1995; Prabu, 1997).

Since the number of outputs after combining the array reduces by a factor of 30, one can afford to demultiplex the two polarization channels onto two parallel transmission links. Thus the data sent forward from the GAC into the pulsar receiving system will have the form and sequence as shown in figure (1.6). There will be four parallel transmission links in each sub-band corresponding to the real and imaginary parts of two polarizations of the combined array. The data of consecutive FFT spectra appear on these channels at a rate of 16 mega samples /sec. To provide for the growth in the number of bits during array summation, the data on these channels are represented by 10 bit wide for parallel transmission of all the bits. A timing clock associated with this data is also transmitted in parallel for clocking all the back end systems such as the pulsar receiver. An additional signal is also transmitted in parallel to indicate when valid data is being transmitted on the links, so that the back end systems can perform other tasks during those clock intervals when valid data is not available.

1.7. Overview of the ORT (Ooty Radio Telescope):

The ORT, operating at 327 MHz, is a radio telescope located in Ootacamund, Tamil Nadu, India. It is in operation since about 30 years and has provided a highly useful tool for low frequency radio astronomy.

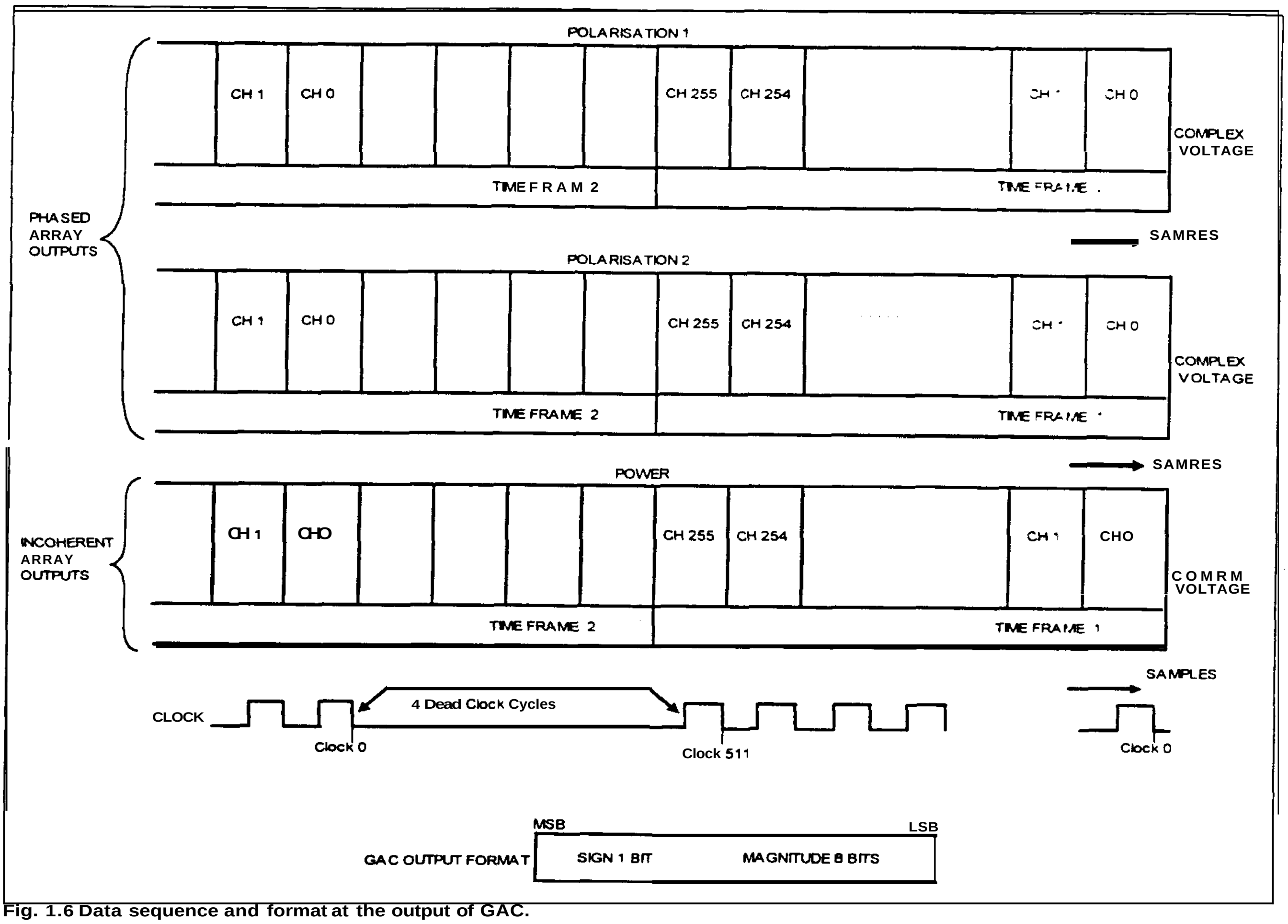

Fig. 1.6 Data sequence and format at the output of GAC.

1.7.1. Front-end System:

A block diagram of the RF front-end of ORT is shown in figure (1.7). It consists of a parabolic cylindrical reflector of 30m wide in east-west direction and a length of about 500m in the north-south direction (Selvanayagam A.T. 1993). An array of 1056 dipole feeds placed at the focus collects the radiation reflected off the parabolic cylinder. The entire cylinder can be mechanically rotated to track a source as the earth rotates for about 9 hours. The dipoles are arranged in the north-south direction, and voltages received within a set of every 48 adjacent dipoles is summed

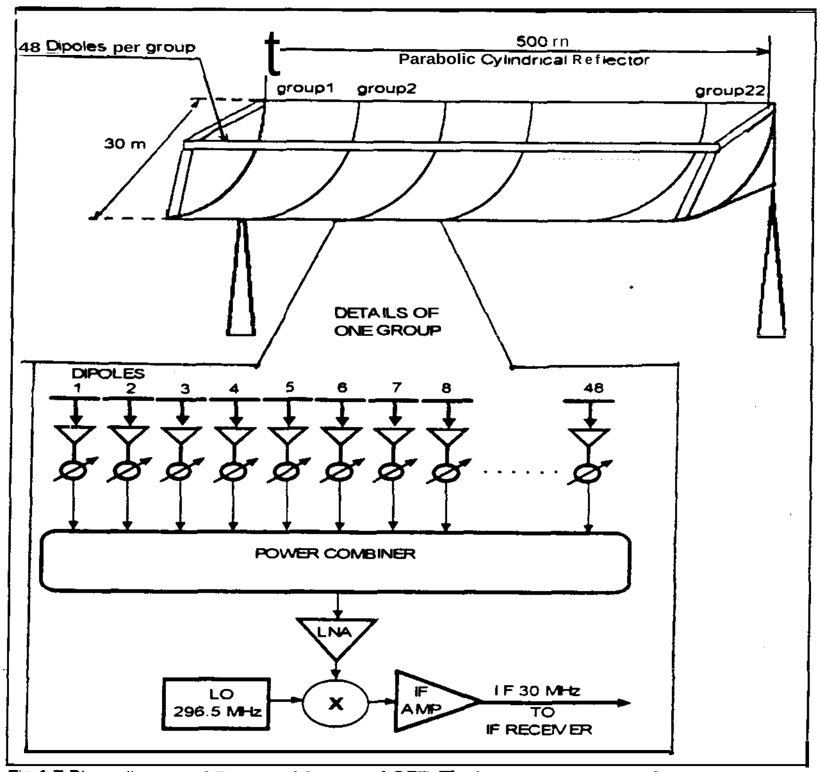

Fig 1 7 Block diagram of Front-end System of ORT The lower block repeats for every group of the parabolic cylinder aray up using analog power combiners right at the dipole feeds. Before summing, the phase differences between the signals of the dipoles within each group due to differences in arrival times are compensated using programmable analog phase shifters. Depending on the direction to which the response is to be maximized along the north-south direction, the setting of the phase shifter is suitably changed. After summing, there are 22 groups, each with a band of about 20 MHz, centered around 327 MHz. With the given bandwidth and proximity of the dipoles within a group, the arrival time differences between dipoles of a group are small enough so that only phase compensation is done (no delay compensation). The signals of each group are mixed with a coherent local oscillator signal to down-convert each of these RF bands to IF bands of 30 MHz, which makes it easier to transmit them via coaxial cables to a central building where further processing continues.

1.7.2. IF and Base Band System:

Figure (1.8) shows the layout of the IF and base-band sections at the control center of ORT. The 22 groups need to be combined after phasing the array. Since the distance between groups is large, the signals

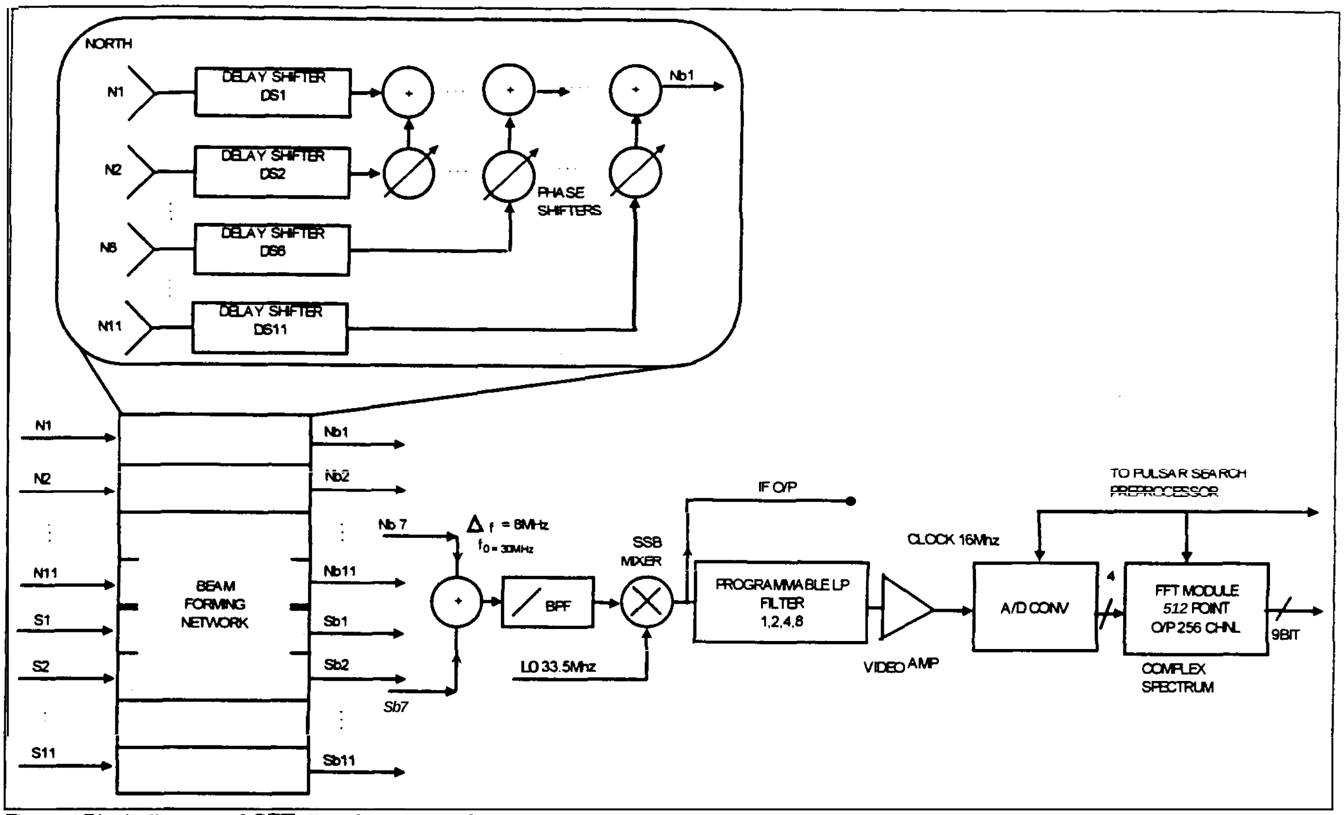

Fig. 1.8 Block diagram of ORT IF and Base-Band system.

are passed through programmable analog delay lines, which compensate the differential delays and phases between them. As with the RF phase shifters, delay shifters are programmed suitably depending on the declination to which the array response has to be maximized. After compensation, the signals from all groups are passed through twelve sets of phase shifters and summers, which produce 12 simultaneous beams of the telescope, each pointed about 6 arc-minutes away in declination from the next. The combined response of each beam will then have a beam-width of 6'arc X 2°, and the direction can be steered electrically to different declinations and mechanically point at different hour-angles. This is to facilitate concurrent, multi beam observations which are useful in conducting surveys of the sky. In our experiments only one of them (the center beam) is tapped.

The bandwidth of the each combined IF signal is restricted to about 8 MHz and passed to SSB mixers which convert the IF bands to video bands with an option to choose the base-band width between 1, 2, **4,** or 8 MHz. The signal in the selected band then passes to a set of **A/D** converters. The sampling speed is programmable so that for lower bandwidths, one can sample slower, just enough to ensure Nyquist sampling rate. The sampler is followed by a FFT module. Both the sampler and FFT module are same as that for the GMRT, except that they run at a maximum speed of 16 Msamples per second. An array combiner module is used just to interface the **FFT** to the Pulsar signal processor and present the data in the order and sequence discussed earlier.

The telescope provides a collecting area of about 8000 sq **.m.** and front-end noise temperature of about 150°K. These along with its bandwidth of 8 MHz make it possible to reach a detection levels of about a milli Jansky for observations of pulsars over about 10 minutes. One of the major advantages of this telescope is that the slope of the hill on which the telescope lies parallel to earth's rotation axis, thus making the telescope free from any polarization changes due to parallactic angle. However, the telescope is a single polarization array and is limited in this sense for polarization observations of pulsars. However, for some pulsars, an alternate technique as discussed in chapter 5 can be used to get polarization information by choosing different portions of the frequency band, where the Faraday rotation in the ionosphere would have rotated the other hand of polarization to align with that of the telescope.

1.8. Layout of the Thesis

The work presented in this thesis describes the design and development of a real-time signal processing receiver to be used in the search and study of pulsars. Various pulsar signal processing instruments already existing have been designed to serve a specific class of pulsar observations, such as pulsar timing observations **(Steinberg** et. al, **1992),** Dynamic spectra studies (Backer et. al., **1990),** etc, In many cases, existing hardware (built for other observations) have been used with some modifications for pulsar observations, obviously making compromises in spectral or temporal resolution of data. Although a hardware system built specifically for a specific type of pulsar observation may prove to be functionally better, it is often too expensive a solution to build special purpose instruments for every other type of observation. In some cases, the polarization information is sacrificed to save on the hardware. In the planning for GMRT, the need was felt for developing a general purpose pulsar signal processing spectrometer with 512 frequency channels, that is capable of estimating full polarization information (total power, linear and circular components) across a bandwidth of **32MHz.** The instrument is required to handle one or more of any of the corrections such as incoherent de-dispersion, Faraday de-rotation, Doppler acceleration compensation, Synchronous pulse folding, variable integration in frequency and time, windowed gating of on-pulse regions. It is designed to handle various observations ranging from single pulse measurements to long term folded average profiles over several minutes, and cover the entire parameter space of pulse period, width, strength, polarization and dispersion, with a maximum time resolution of 16 microseconds. Table 1.1 summarizes the

PERFORMANCE OF DIFFERENT PULSAR RECEIVER SYSTEMS.

Table (1.1 a)

Sl. No	No.Polari-Sation Channels t,L,C total power = t linear = L circular = C	No.of input Channels (Nch in)	Minimum Raw sampling Interval word width	Frequency Averaging (Nchout)	Boxcar averaging Nint(Max)	Max No. of period folds (Nfolds), Max No. of bins across one period.(Nbins)	Dedispersion	
							Incoherent	Coherent
1	Steinberg. et.al (1992)	1 to 32	2.8x10 = 36nsec to Nchin 12.8μsec 6 bits	Nchout=Nchin	1 to 255 samples	1 to 65536 periods, $\left(\frac{32768}{\text{Nchout}}\right)$	0.34 with 32 channels @ 1420 MHz	--
2	This System t,L,C	512	16μsec in all channels, 9 bits	Nchout=16 to 512, (Output freq.channels) (1 to 32 adjacent channels collapsable per output channel)	1 to 16M samples	1 to (16M-Nint) periods, $\left(\frac{\text{512K}}{\text{Nchout}}\right)$	0.2 with 512 channels @ 1470 MHz	--
3	Backer.et.al (1989)	64	25μsec – fastmode 250μsec – search mode 12 bit	Nchout=Nchin	1 to 8 samples	- -	---	0.2 with 64 channels
4	(Deshpande, et.al.1992) t	128	2 msec (8 bits)	Nchout=Nchin	1 to 128 samples	--	---	3 with 128 channels
5	(Van Ommen) 1992 . L	16	1 μsec 4,8 or 12 bits	Nchout=Nchin	64K, 4K, 256 respectively with initial word width	1024 bins $\left(\frac{\text{1to65536periods}}{\text{Nint}}\right)$	--	--

Table (1.1 **b**)

SL No.	Technology: Computation Logic	Technology: Control .Logic	Doppler Acceleration Correction interval & maximum resolution	Total Bandwidth best frequency resolution	Pulse Gating	Parallactic Angle Correction	Faraday Rotation Correction	Data Recording Rate
1	Discrete TTL	PROM based State machine	Once every second 1 part in 10^9	1.4 MHz 44 KHz	Single Window across all channels	—	–	Processing pauses for a few seconds during result recording of every set of folds
2	FPGAs, PROM Lookup tables DSP chips	FPGA state Machine	Whenever error is $\left(\frac{\text{Binwidth}}{4}\right)$ $\left(\frac{Sampint}{4X10^9}\right)$	32 MHz 64 KHz	Independent Windows for each channel	Once every second	512 point resolution across chosen bandwidth. accuracy limited by Telescope sensitivity	Programmable from 8Mbytes/sec to slower rates. local PC Acqu. Upto 128 Kbytes/sec continuous acquisition. (Without interrupting processing)
3	Discrete logic Autocorrelator (Arecibo Observatory)	µp based board	Once every second Not available	40 MHz 620 KHz	--	—	–	Multibus based Tape recorder 128Kbytes/Sec
4	Existing Autocorrelator +TTL Logic +Analog Sweeping LO System	Discrete TTL Logic	--	1 MHz 8 KHz	--	–	–	Discrete logic interface to tape recorder. Max. rate of 128 Kbyteslsec
5	ALU	µp based Controller	Once every period (resolution 1µsec)	8 MHz 512 KHz	Single window for all channels	--	–	VAX 1170 based tape recording Max. of 16 Kbytes/sec

comparison of various aspects of the instruments available at the time of design. The main problem posed in the design of such a system is to deliver the required real-time computational throughput without loss of precision in the data and providing simple means of configuring the system functions for a given type of pulsar observation.

In the next chapter, titled **DESIGN OPTIMIZATIONS,** several considerations that came up during the design of the system are discussed. These include the signal processing algorithms required for real-time cleaning of the received signals from distortions due to dispersion, Faraday rotation, Doppler acceleration, and improving signal to noise ratio using the statistical nature of the received signals. Optimizations in signal processing methods are discussed and the development of a single algorithm to perform all the correction functions so as to simplify the computation and data communication requirement are presented. The later half of the chapter highlights the engineering challenges that the design of such a system poses, and possible short-cuts and simplifications that were worked out during the design.

After these optimizations were worked out, it became clear that there was a need for two types of on-line pre-processing systems: one which was specially tuned to GMRT (and ORT) requirements to be used for deep search and study of pulsars and the other, a light portable receiver which could be taken around to any telescope for some pulsar studies over a smaller, limited band-width. Based on these designs, prototype systems were developed and tested in the lab using several diagnostic methods. Systems for which all tests were completed successfully were then moved to the ORT /GMRT site and are commissioned at these telescopes. Trial observations were then conducted on actual pulsars to identify all systematic .errors that would show up with the processing of the weak pulsar signals. The feedback from these field tests are being used to improve the system performance. Since the volume of work involved in the development and testing of all these machines is quite large, the testing of different parts of the overall system are in various stages, some have been successfully used for observing pulsars since 1993, some parts are undergoing field test presently. In **chapter three,** titled PULSAR SEARCH PRE-PROCESSOR (PSP), design, tests and results of the PSP and a Portable Pulsar Receiver are discussed.

The design, tests and results of an instrument built for pulsar studies is presented in **chapter four,** titled SIGNAL PROCESSOR FOR PULSAR STUDIES (SPPS). The architecture of the polarimeter and Digital Signal Processor (DSP) based parallel-processing system which form the SPPS is explained. Hardware and software optimizations in the implementation of the signal processing algorithms are discussed. The strategy for distribution of code/data to different nodes of the DSP parallel processor is described. Implementation of a high-speed PC-based data recording system built for collecting the results from the SPPS is also explained. The design and implementation of Fast-Fourier-Transform module built for testing the SPPS is explained. Tests conducted and corresponding results are presented.

In the process of deciding the accuracy of various parameters that the signal processor would use, it was necessary to find the inherent uncertainities in the Faraday rotation contribution due to the ionosphere, which would, at times become highly turbulent. While trying to figure out a method to possibly estimate and adaptively correct for the RM changes that this would introduce, a novel method of using pulsars themselves as probes of the ionosphere was developed. Since the only telescope available close to GMRT having sufficient sensitivity was the ORT, an improved method of conducting polarization observations with a single polarization telescope was evolved. Trial observations were successfully conducted. The techniques along with the first successful results are presented in **chapter five,** titled **NEW SIGNAL PROCESSING METHODS FOR ESTIMATION OF PULSAR ROTATION MEASURE.**

In **chapter six,** titled **DISCUSSION & CONCLUSION,** the current status and future scope of work are summarized. Even though the signal processing system is designed primarily for pulsar work, some parts of this machine will be highly useful in many other signal processing applications. Some of such applications are highlighted towards the end of this chapter.